Impact of Orbital Parameters and Greenhouse Gas on the Climate of MIS 7 and MIS 5 Glacial Inceptions

FLORENCE COLLEONI

Centro Euro-Mediterraneo sui Cambiamenti Climatici, Bologna, Italy

SIMONA MASINA AND ANNALISA CHERCHI

Istituto Nazionale di Geofisica e Vulcanologia, Sezione di Bologna, and Centro Euro-Mediterraneo sui Cambiamenti Climatici, Bologna, Italy

DOROTEACIRO IOVINO

Centro Euro-Mediterraneo sui Cambiamenti Climatici, Bologna, Italy

(Manuscript received 7 December 2013, in final form 9 September 2014)

ABSTRACT

This work explores the impact of orbital parameters and greenhouse gas concentrations on the climate of marine isotope stage (MIS) 7 glacial inception and compares it to that of MIS 5. The authors use a coupled atmosphere–ocean general circulation model to simulate the mean climate state of six time slices at 115, 122, 125, 229, 236, and 239 kyr, representative of a climate evolution from interglacial to glacial inception conditions. The simulations are designed to separate the effects of orbital parameters from those of greenhouse gas (GHG). Their results show that, in all the time slices considered, MIS 7 boreal lands mean annual climate is colder than the MIS 5 one. This difference is explained at 70% by the impact of the MIS 7 GHG. While the impact of GHG over Northern Hemisphere is homogeneous, the difference in temperature between MIS 7 and MIS 5 due to orbital parameters differs regionally and is linked with the Arctic Oscillation. The perennial snow cover is larger in all the MIS 7 experiments compared to MIS 5, as a result of MIS 7 orbital parameters, strengthened by GHG. At regional scale, Eurasia exhibits the strongest response to MIS 7 cold climate with a perennial snow area 3 times larger than in MIS 5 experiments. This suggests that MIS 7 glacial inception is more favorable over this area than over North America. Furthermore, at 239 kyr, the perennial snow covers an area equivalent to that of MIS 5 glacial inception (115 kyr). The authors suggest that MIS 7 glacial inception is more extensive than MIS 5 glacial inception over the high latitudes.

1. Introduction

Over the last 5 million years, Earth's climate experienced two major transitions. The first one occurred at the end of the Pliocene, ≈3.3–2.7 million years (Myr) ago (e.g., Haug et al. 2005; Mudelsee and Raymo 2005), when the ice sheets started to develop over the Northern Hemisphere. The second one occurred roughly 1 million years ago when the frequency of the glacial/interglacial cycles evolved from a 40- to a 100-kyr frequency (e.g., Lisiecki and Raymo 2007). During the last decades, the analysis of ice cores and marine sediment records revealed that another threshold in global climate occurred toward 430 kyr, the so-called Mid-Brunhes Event (MBE; e.g., Jansen et al. 1986). The proxy records show that the interglacials that occurred before this event were less intense than for the last past five interglacials. Marine isotope stage (MIS) 7 (≈245–190 kyr) seems, however, to be an exception.

In a recent study, the comparison between $\delta^{18}O$ and CO_2 concentrations shows that MIS 7 could be considered as a cold interglacial: that is, more similar to the pre-MBE interglacials than to the post-MBE ones (Tzedakis et al. 2012). Pre-MBE interglacials are characterized by low sea level and probably larger Northern Hemisphere ice sheets (Helmke et al. 2003), particularly low CO_2 concentrations (Luthi et al. 2008), and no CO_2 overshoots (Tzedakis et al. 2012). Recent reconstructions

Corresponding author address: Florence Colleoni, CMCC, Viale Aldo Moro, 44, 40127 Bologna, Italy.
E-mail: florence.colleoni@cmcc.it

DOI: 10.1175/JCLI-D-13-00754.1

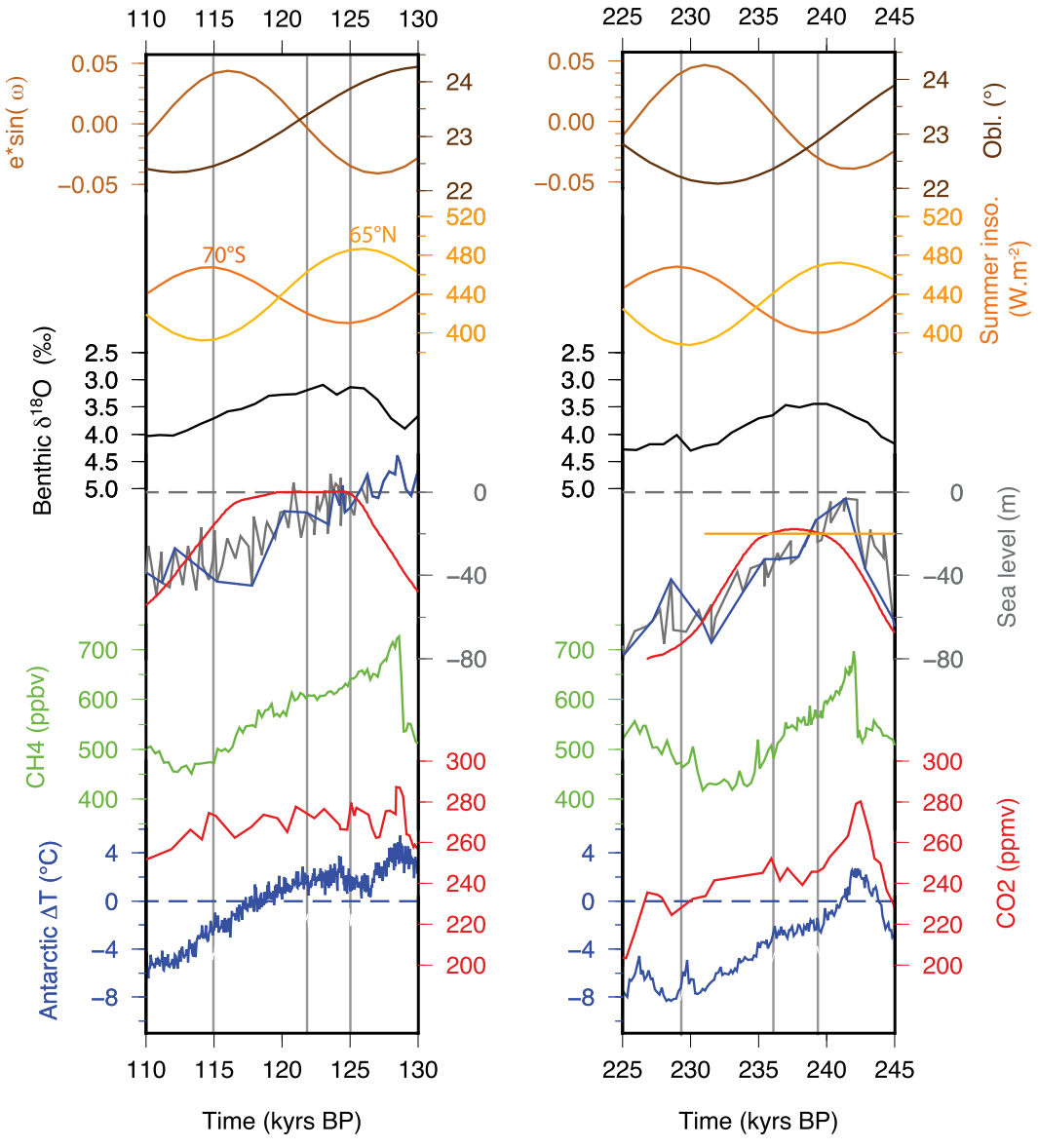

FIG. 1. Close-up of (left) MIS 5 and (right) MIS 7 interglacials illustrated by different external forcing and climate proxies: (top)–(bottom) obliquity (°; dark brown) and precession index (Berger 1978; light brown); summer insolation at 65°N and 70°S ($W\,m^{-2}$; Berger 1978; light and dark orange, respectively); benthic $\delta^{18}O$ stack record (Lisiecki and Raymo 2005); sea level reconstructions (m) from Rohling et al. (2009) (gray), Siddall et al. (2006) (blue), and Bintanja et al. (2005) (red) and constraint on global mean sea level by Dutton et al. (2009) (orange); atmospheric CH_4 (ppbv; green) and CO_2 (ppmv; red) concentrations from European Project for Ice Coring in Antarctica (EPICA) Dome C, East Antarctica (Loulergue et al. 2008; Luthi et al. 2008); and EPICA Dome C temperature anomaly (°C) relative to present day (Jouzel et al. 2007; blue). Vertical gray bars indicate the time of the climate snapshots simulated in this work.

suggest indeed, that MIS 7 sea level stayed between 10 and 20 m below present-day level (Fig. 1; Dutton et al. 2009). However, the atmospheric concentration of greenhouse gas (GHG) recorded in East Antarctica exhibits an overshoot at MIS 7 peak interglacial (≈245 kyr) before dropping abruptly to levels comparable to pre-MBE interglacials (Fig. 1; below 260 ppm). In fact, after 245 kyr, CO_2 concentration drops below 240 ppm in less than 10 kyr, while for MIS 5, as an example of post-MBE interglacials, CO_2 remains above 260 ppm for almost 20 kyr (Fig. 1). Similar variations are also observed in the CH_4 concentration from the East Antarctica ice-core record, which shows a substantial drop during MIS 7 (Fig. 1). Furthermore, East Antarctica mean annual

TABLE 1. Climate experiments settings. Three sets of simulations were carried out: $MIS5_{FULL}$ and $MIS7_{FULL}$ correspond to experiments forced using the proper orbital parameters and greenhouse gas concentrations from the MIS 5 and MIS 7 periods, respectively, and MIS7_GHG experiments were forced using MIS 7 orbital parameters but MIS 5 GHG values. GHG were retrieved from EPICA Dome C and come from Luthi et al. (2008) for the CO_2 records, Loulergue et al. (2008) for the CH_4 records, and Schilt et al. (2010) for the NO_2 records. Orbital parameters are calculated according to Berger (1978). For the preindustrial control experiment CTR1850, orbital parameters were set to 1990 while the GHGs were set at their preindustrial values (1850). Finally, K115 and K122 experiments were initialized from the 400th model year of K125 while the K229 and K236 simulations were initialized from the 400th model year of K239.

Set	ID (%)	Eccentricity date	Perihelion (°)	Obliquity (ppm)	CO_2 (ppb)	CH_4 (ppb)	NO_2	Spinup	Length (model years)
$MIS5_{FULL}$	CTR1850	0.017	4 Jan	23.44	284	791	275	Preindustrial	700
	K115	0.042	14 Jan	22.44	262	472	251	K125 branch	300
	K122	0.041	12 Sep	23.33	274	607	257	K125 branch	300
	K125	0.040	23 Jul	23.80	276	640	263	—	700
$MIS7_{FULL}$	K229	0.043	3 Feb	22.22	224	493	256	K239 branch	300
	K236	0.038	2 Oct	22.23	241	481	267	K239 branch	300
	K239	0.036	12 Jul	22.70	245	565	267	K239 branch	700
MIS7_GHG	K229_GHG	K229	K229	K229	262	472	251	K239 branch	300
	K236_GHG	K236	K236	K236	274	607	257	K239 branch	300
	K239_GHG	K239	K239	K239	276	640	263	—	700

temperature anomaly record (Jouzel et al. 2007) suggests that air temperatures during MIS 7 are colder than at the beginning of the other post-MBE interglacials (Fig. 1).

Because of MIS 7 unusual characteristics, literature about its climate is scarce and only focuses on the interglacial aspects of this period (e.g., Yin and Berger 2012). From a glacial inception point of view, one of the rare contributions is that by Colleoni et al. (2014), who use an ice-sheet model to show that MIS 7 cold climate is more favorable to glacial inception than MIS 5 climate over Northern Hemisphere high latitudes, especially over Eurasia. Given the rapid climate evolution toward cold conditions, the timing and amplitude of glacial inception that follows MIS 7 interglacial might be influenced by those cold conditions. However, in Colleoni et al. (2014), the impact of the most exceptional feature of MIS 7 on glacial inception (i.e., the low GHG values) has not been isolated.

The impact of external forcing and of GHG on the high-latitude climate has been extensively investigated in the context of glaciations and glacial inceptions. For example, Wang and Mysak (2002) and Calov et al. (2005) use an Earth system model of intermediate complexity coupled to an ice-sheet model to show that a large drop in summer air temperature is a necessary condition for glacial inception. Several studies (e.g., Kubatzki et al. 2006; Bonelli et al. 2009) suggest that the timing and the amplitude of glacial inception is affected by the degree of synchronicity between insolation minimum and the drop in GHG. Bonelli et al. (2009) further show that, while a decrease in high-latitude summer insolation is sufficient to trigger glacial inception over North America, a drop in atmospheric CO_2 is necessary to trigger a long-lasting glaciation over Eurasia. Finally, Vettoretti and Peltier (2003) show that, for CO_2 values ranging from 260 to 290 ppm (typical glacial inception–interglacial values) and a range of orbital parameters close to those of the last five glacial inceptions, the impact of CO_2 on perennial snow is more or less similar to that of orbital parameters. Nevertheless, they obtain the thickest continental snow cover for the lowest CO_2 concentration and the less contrasting orbital configuration from seasonal point of view (lowest eccentricity and obliquity), which, in their study, corresponds to MIS 7 glacial inception. However, they used a CO_2 value almost similar to the one of the last glacial inception (i.e., ≈260 ppm), therefore missing the effect that the particularly low GHG recorded during the early MIS 7 (i.e., ≈224 ppm; Fig. 1 and Table 1) combined with MIS 7 orbital forcing might have on the timing and the intensity of MIS 7 glacial inception.

The two main objectives of this study are to simulate the climate of MIS 7 glacial inception and to quantify the individual impact of low GHG values and orbital parameters. In the present study, we use a coupled atmosphere–ocean general circulation model to simulate the evolution of MIS 7 climate from interglacial to glacial inception, particularly at 239, 236, and 229 kyr. To better stress the impact of low GHG and orbital parameters on the inception processes, MIS 5 mean climate state is also simulated at 125, 122, and 115 kyr and compared to that of MIS 7. In addition to those simulations and in order to fully capture the impact of the low GHG values on MIS 7 glacial inception, a set of three simulations accounting for MIS 7 orbital parameters and MIS 5 GHG values are carried out. Such simulations are useful to understand the individual impact of GHG on climate since Vettoretti and Peltier (2003) show that the intensity

of a glacial inception depends on the degree of synergy between orbital configurations favorable to glacial inception and low GHG.

This paper is structured as follows: In section 2, we describe the AOGCM used and the experimental setup. In section 3, we describe and discuss the results separating the impacts of GHG and insolation on the northern high-latitudes climate, while in a second time we describe their impact on the perennial snow cover. Finally, section 4 contains the main conclusions of the study.

2. Methods

a. CESM

We use the Community Earth System Model (CESM) version 1.0.5, a fully coupled atmosphere–ocean–sea ice–land model (Gent et al. 2011). The atmospheric component, the Community Atmosphere Model (CAM), has 26 vertical levels and a horizontal grid of 96 × 48 (T31) shared with the land component, the Community Land Model (CLM). The ocean component [Parallel Ocean Program (POP)] has 60 vertical levels and a nominal 3° horizontal resolution in common with the sea ice component [Los Alamos Sea Ice Model (CICE)] with a displaced pole located over Greenland.

1) CESM EXPERIMENTS SETUP

In total, nine experiments are carried out, each representative of different orbital parameters and GHG concentrations characteristic of MIS 7 and MIS 5 periods. The MIS 5 interglacial simulation K125 is spin up to a 125-kyr time period and is used after 400 yr of integration to branch the two experiments K122 and K115 set up with 122- and 115-kyr orbital parameters and GHG values, respectively (Table 1). Similarly, MIS 7 interglacial simulation K239 is spin up to a 239-kyr time period and used to initialize the two runs K236 and K229 set up using 236- and 229-kyr orbital and GHG values, respectively (Table 1). To isolate the effect of the low MIS 7 GHG, three additional experiments have been performed using MIS 7 orbital parameters but MIS 5 GHG values, all branched on the K239 spinup experiment: they are referred to as K239_GHG, K236_GHG, and K229_GHG. These nine simulations have been clustered in three different categories: that is, $MIS5_{FULL}$ for the experiments with MIS 5 orbital parameters and GHG; $MIS7_{FULL}$ accounting for MIS 7 orbital forcing and GHG; and MIS7_GHG accounting for MIS 7 orbital parameters and MIS 5 GHG. Those experiments are defined such that the comparison between $MIS7_{FULL}$ and MIS7_GHG shows the impact of GHG only, the comparison between MIS7_GHG and $MIS5_{FULL}$ shows the impact of orbital parameters only, and the comparison between $MIS7_{FULL}$ and $MIS5_{FULL}$ gives the difference between the two glacial inceptions by combining the impacts of GHG with orbital parameters. The detailed settings are summarized in Table 1. To these experiments, we add a control run (CTR1850) forced with preindustrial orbital parameters set at 1990 and GHG values set at AD 1850 for comparison with the other paleo simulations. All the experiments are 700 model years long, which allows them to almost reach equilibrium in the ocean intermediate water (not shown). Although a slight drift in oceanic heat content still persists in the experiments because of the abyssal circulation, we assume that it is small enough to not affect our main conclusions (not shown; Jochum et al. 2012).

2) CESM PERFORMANCES

As shown in Jochum et al. (2012), Shields et al. (2012), and Colleoni et al. (2014), the low-resolution CESM is affected by a weak North Atlantic ocean heat transport toward high latitudes of 0.66 PW instead of ≈1.2 PW as suggested by present-day observations (Yeager et al. 2006, and references therein). This causes large negative air temperature and precipitation biases over northern Eurasia in the simulated present day. Despite the impact that such a cold bias might have on glacial inception processes, no ice sheet grows in the preindustrial climate simulation CTR1850 (Colleoni et al. 2014). This gives more confidence to the results that will be discussed in the next sections.

To check back in time if this bias could affect our simulated climates up to MIS 7, we compare our experiments to some of the available paleo sea surface temperature (SST) reconstructions and to high-latitude ice-sheet reconstructed past temperatures (Fig. 2). The sites that we selected for our comparison are detailed in the caption of Fig. 2 and are taken from Dahl-Jensen et al. (2013) for Greenland, from Kawamura et al. (2007) and Jouzel et al. (2007) for Antarctica, and from Lang and Wolff (2011) for the marine sites. In the North Atlantic, north of 50°N, the differences between modeled and observed SSTs are negative for all the experiments (squares in Fig. 2). These discrepancies are on the order of −7°C and slightly less for K125 and K122 (≈−4°C) and can be associated with the cold bias identified in Northern Hemisphere high latitudes due to a lack of ocean heat transport in the low-resolution version of CESM. In the other basins and in all the experiments, except in K125, the absolute SSTs differences are on the order of 1°–2°C. K125 shows peculiar characteristics: the model globally underestimates SSTs observations by about 2°–4°C, probably because of the cold bias inducing a southward

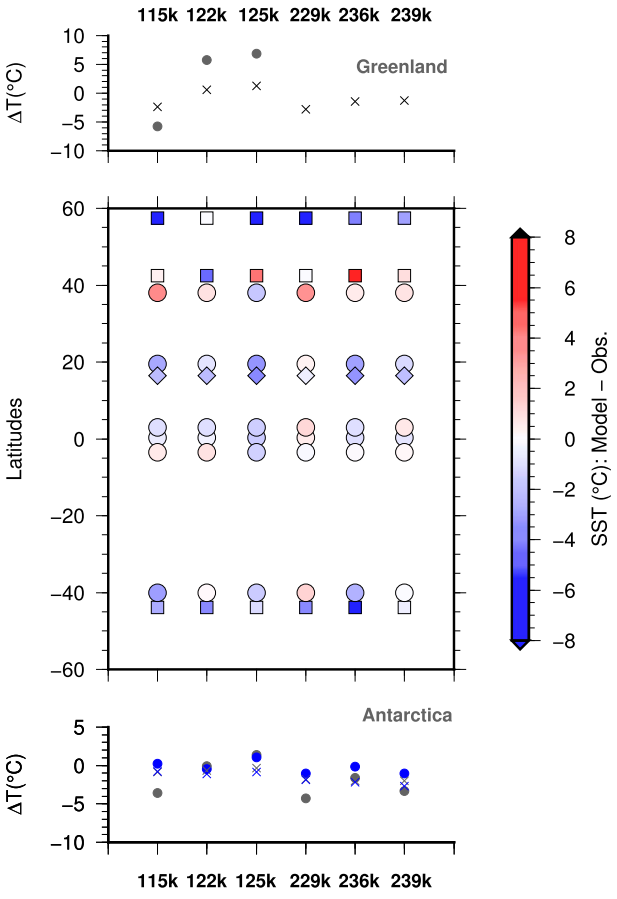

FIG. 2. Simulated air and SST compared with proxy data. (top) Greenland air temperature differences (°C) relative to preindustrial period at the North Greenland Ice Core Project (NorthGRIP) site (≈83°N). Crosses correspond to modeled values, while solid circles correspond to air temperature differences retrieved from the NorthGRIP ice core record (Johnsen et al. 2001). Note that NorthGRIP record does not reach MIS 7 time period. (middle) Differences between simulated and observed SST over latitudes. Atlantic sites are indicated by squares, Pacific sites are marked with circles, and the only Indian site is shown by a diamond. See Lang and Wolff (2011) for the description of the marine sites considered in the comparison. (bottom) As in (top), but for Antarctica. Two sites are considered for comparison: the Dome Fuji ice core record (Kawamura et al. 2007; gray) and the EPICA Dome C ice core record (Jouzel et al. 2007; blue). Simulated values, both for marine and terrestrial sites, correspond to the average of the six closest grid points surrounding the location of each observed site.

deviation of the westerlies combined to a southward shift of the ITCZ larger than what the data suggest. However, as it will be described in section 3, this does not have consequences in terms of glacial inception. Over Antarctica, all the experiments underestimate temperature reconstruction from Dome C by about 2°C but overestimate the Dome Fuji temperature record by about 2°C. Over Greenland, K115 slightly overestimates temperatures while K125 and K122 are too cold (≈3°C). Note that, over both Greenland and Antarctica, MIS 7 simulations are colder than MIS 5 ones. It is also worth noting that no data are available to compare with MIS 7 experiments since Greenland ice history does not extend beyond the Eemian interglacial time period (≈130 kyr).

b. *MIS 5 and MIS 7 orbital configuration*

The evolution of insolation from K239 to K229 is highly similar to that from K125 to K115. However, because of low eccentricity values at K239 and K236 (Table 1), the seasonal contrast is less pronounced during MIS 7 than during MIS 5. As a result, the insolation difference between K239, K236, and K229 is smaller than between K125, K122, and K115 (Figs. 3a–f). Perihelion occurs at mid-July in K125 and at late July in K239, but obliquity and eccentricity are both larger in K125 than in K239 (Table 1), which explains why summer insolation in K125 is larger than in K239 (Table 1). The precession is almost similar between K236 and K122, with perihelion occurring in the middle of September and early October, respectively (Figs. 3b,e). Similarly to K239 and K122, the discrepancy between K236 and K122 is explained by the larger obliquity and eccentricity values, which induces a larger insolation in K122 (Fig. 3h). In K229 and K115, which both correspond to the orbital time of glacial inception for both MIS 7 and MIS 5, perihelion occurs in mid-January and early February, respectively (Fig. 3g). Above 60°N, summer insolation is slightly lower, by about 10 W m^{-2}, in K229 than in K115 (Fig. 3g). Obliquity is similar and at its minimum in both simulations, while eccentricity is slightly larger in K229 than in K115 (Table 1). The fact that perihelion in K229 occurs in early February with a particularly low obliquity means that boreal summer occurs almost at aphelion and that the seasonal contrast between boreal winter and boreal summer is reduced. Finally, the discrepancy in insolation observed during northern high-latitude fall between K229 and K115 results from the difference in precession between those two time periods.

3. Results

a. *Comparison of MIS 7 and MIS 5 seasonal cycle*

Most of the orbital characteristics described in the previous section have a strong influence on the high-latitude climate. In MIS5$_{\mathrm{FULL}}$ experiments, the temperature difference between the interglacial simulation K125 and K122 is smaller than between K125 and K115 during winter (Figs. 4a,b) as well as summer (Figs. 4c,d). As a consequence of the precession, during winter, K122

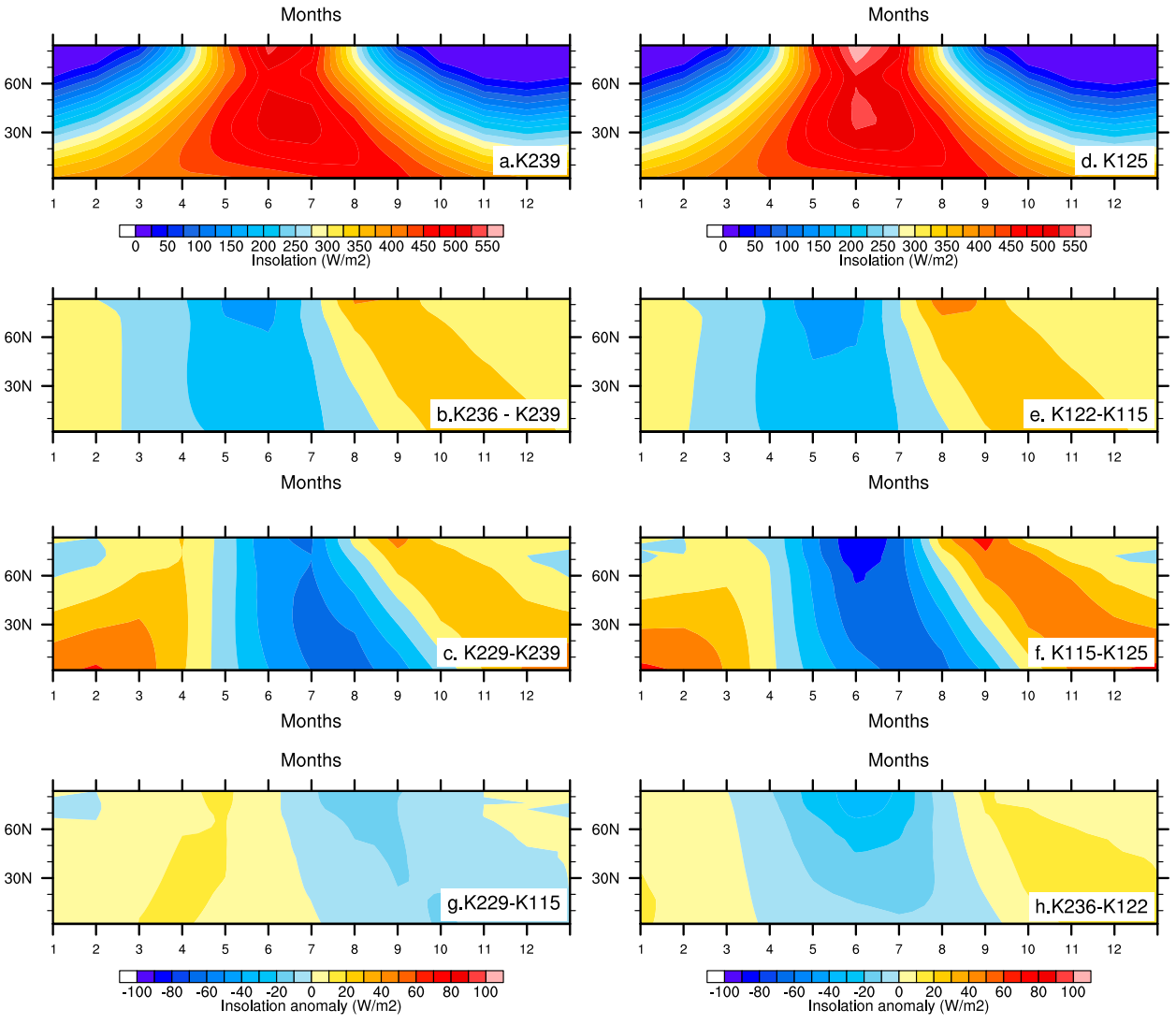

FIG. 3. Annual cycle of incoming solar downward radiation at the top of the atmosphere ($W\,m^{-2}$) over the Northern Hemisphere. The differences in insolation are shown between interglacial simulations and the other simulated time slices: (a) K239, (b) insolation difference between K236 and K239, (c) difference between K229 and K239, (d) K125, (e) difference between K122 and K125, (f) difference between K115 and K125, (g) difference between K229 and K115, and (h) difference between K236 and K122. See Table 1 for more details on the orbital configurations.

and K115 exhibit temperatures up to 6°C or more larger than in K125. Note that a negative temperature difference of about −2° to −6°C is simulated over the Arctic Ocean in K122 and K115 with respect to K125. This is the effect of a substantial thickening of the sea ice cover combined to the accumulation of a perennial snow layer on the top of it, which increases the local albedo and therefore decreases local temperatures (not shown). Opposite to winter and as a consequence of precession, K122 and K115 exhibit summer temperatures 6° lower than in K125 (Figs. 4c,d).

Similarly to $MIS5_{FULL}$, in $MIS7_{FULL}$ experiments the temperature difference between the interglacial simulation K239 and K236 is smaller than between K239 and K229 during both winter and summer (Figs. 4e–h). In K236 and K229, precession causes winters and summers to be up to 4°C warmer and colder than in the interglacial simulation K239, respectively. Similarly to K122 and K115, a negative temperature difference is simulated over the Arctic Ocean during winter in K236 and K229 as the consequence of the accumulation of a perennial snow cover over the sea ice cover (not shown). However, because of a lower seasonal contrast in $MIS7_{FULL}$ experiments with respect to $MIS5_{FULL}$ experiments, the amplitude of the temperature differences between the interglacial run K239 and the other two runs is smaller.

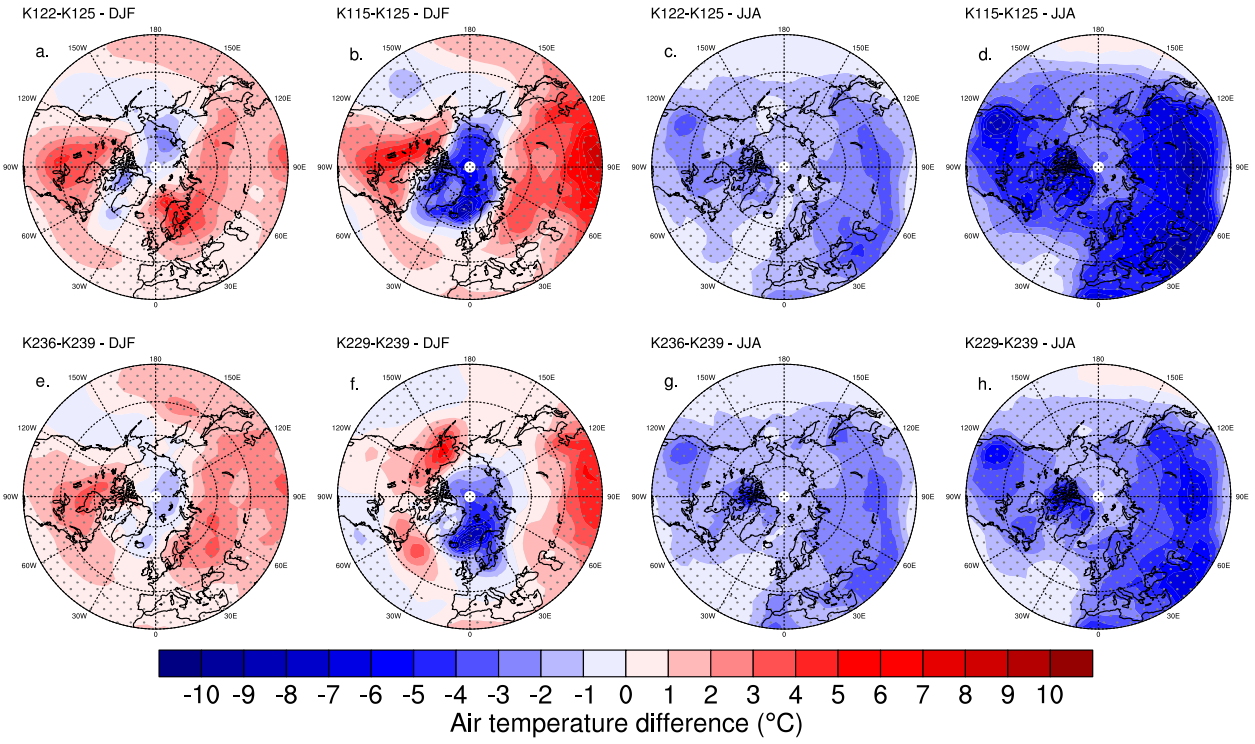

FIG. 4. Mean seasonal air temperature difference over the Northern Hemisphere (°C): (a) K122 − K125 winter difference [December–February (DJF)], (b) K115 − K125 winter difference, (c) K122 − K125 summer difference [June–August (JJA)], (d) K115 − K125 summer difference, (e) K236 − K239 winter difference, (f) K229 − K239 winter difference, (g) K236 − K239 summer difference, and (g) K229 − K239 winter difference. Dotted areas correspond to a *t*-test 95% significance level.

This effect is particularly visible during winter in both K236 and K229 (Figs. 4e,f) and is the consequence of the small difference in eccentricity between K239 and K236, which reduces the seasonal contrast compared to $MIS5_{FULL}$ simulations (Table 1). The seasonal contrast between K239 and K229 is slightly stronger than between K239 and K236 because K229 has the largest eccentricity of the three $MIS7_{FULL}$ time slices. However, the difference in eccentricity between K239 and K229 is compensated by the fact that perihelion occurs during late winter in K229. Therefore, the seasonal contrast between these two simulations is reduced. As a result, winters are not as warm as if perihelion would have occurred close to winter solstice, as for K115. Furthermore, in K229, most of the Eurasian Arctic margin does not exhibit any significant winter temperature difference with K239 (Fig. 4f) because of the impact of the particularly low GHG that counteract the effect of insolation. The impact of GHG is analyzed in more detail in the following sections.

b. *Impact of GHG and orbital parameters on surface air temperature*

Compared to $MIS5_{FULL}$ experiments, $MIS7_{FULL}$ mean annual air temperatures are generally lower by 1°–3°C over the Northern Hemisphere (Figs. 5d–f). Mean annual air surface temperature over the Arctic Ocean is much lower in K239 and in K236 than in their MIS 5 counterparts because the sea ice cover is thicker in $MIS7_{FULL}$ experiments and a perennial snow cover accumulates on top of it (not shown). Both effects contribute to increase the local albedo and therefore decrease local temperatures. The large temperature difference over the Arctic Ocean is reduced between K229 and K115 because they are both glacial inceptions and therefore they present a sea ice cover with similar characteristics (not shown). The difference in mean annual temperature between $MIS7_{FULL}$ and $MIS5_{FULL}$ is on average around −1°C over North America and Eurasia (Figs. 5d–f), except in K239, where Scandinavia exhibits slightly higher temperatures. Despite the fact that K229 and K115 present highly similar insolation, K229 is nevertheless colder by about 1.5°C over a large part of northern Eurasia and North America. This is the experiment presenting the largest negative difference in mean annual temperature over those areas compared to $MIS5_{FULL}$ simulations.

The comparison between MIS7_GHG experiments and $MIS5_{FULL}$ and between $MIS7_{FULL}$ and MIS7_GHG gives the contribution of orbital parameters (Figs. 5g–i)

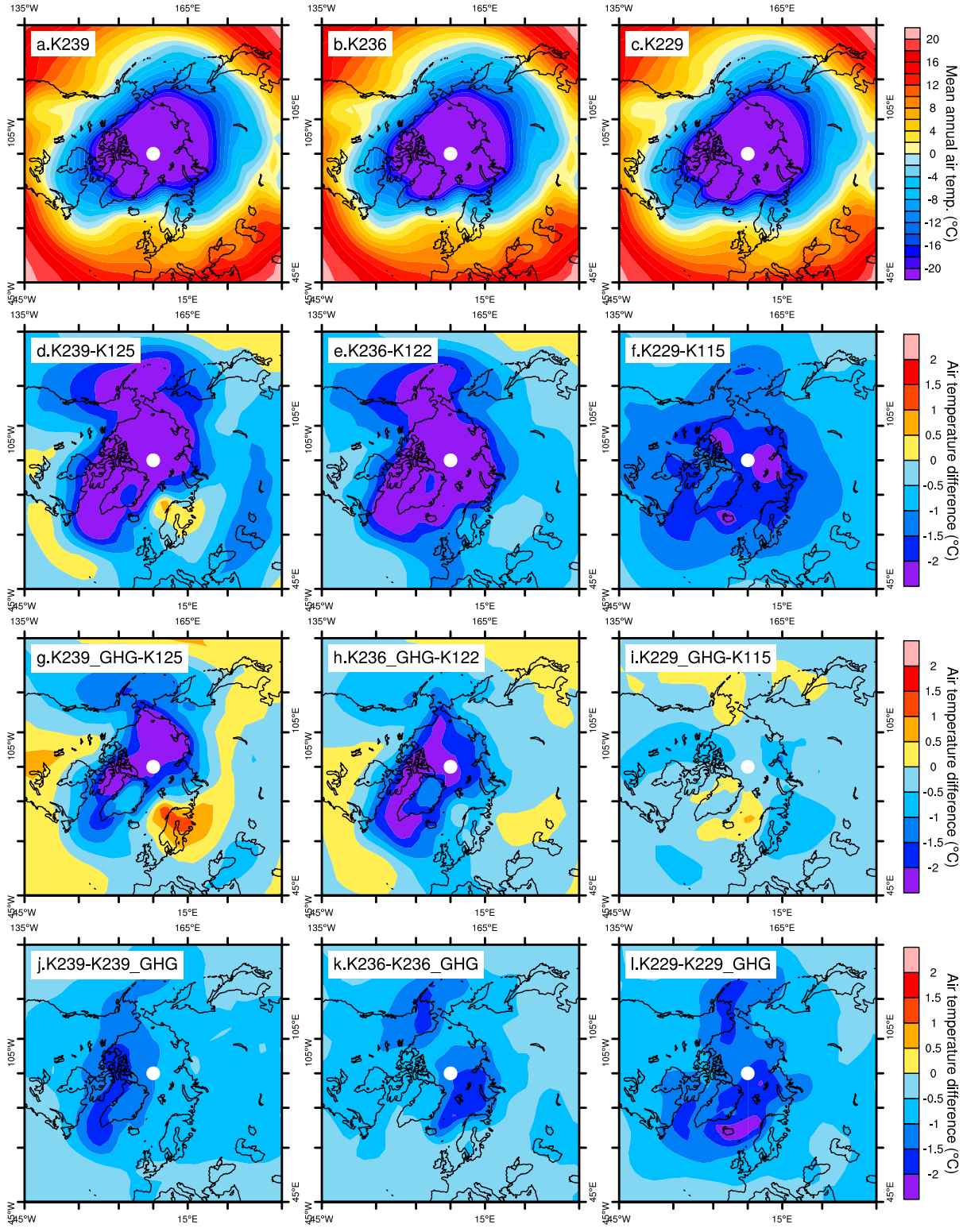

FIG. 5. Impact of orbital parameters and GHG on Northern Hemisphere mean annual air temperature (°C) of the MIS 7 period: (a)–(c) mean annual temperature for K239, K236, and K229 (°C); (d)–(f) difference between MIS 5 and MIS 7 mean annual temperature (°C); (g)–(i) impact of MIS 7 orbital parameters (°C; MIS7_GHG − $MIS5_{FULL}$ experiments; see Table 1); and (j)–(l) impact of MIS 7 GHG (°C; $MIS7_{FULL}$ − MIS7_GHG experiments; see Table 1).

and GHG (Figs. 5j–l) to the mean annual difference between the two periods (Figs. 5d–f), respectively. In K239, insolation induces higher temperatures over Scandinavia (about 1.5°) and over North America (0.5°C). The contribution of orbital parameters becomes negative over Eurasia in K236 (−0.5° to −1°C) and negative over both Eurasia and North America in K229 (Figs. 5h,i). Note that the difference in orbital parameters also explains most of the negative temperatures simulated over the Arctic Ocean (Figs. 5e,h). MIS 7 low GHG induce lower temperatures (about 1°C) over the entire Northern Hemisphere in all the $MIS7_{FULL}$ experiments (Figs. 5j–l). GHG explain about −1.5° to −2°C of the total temperature difference between K239 and K125 (Fig. 5d) over the Canadian archipelago and the Alaska (Fig. 5j). The contribution of GHG is on the contrary more important over the Barents and Kara Seas in K236 (Fig. 5k). In both K239 and K236, the low GHG mostly compensate for the effect of orbital parameters. On the contrary, in K229, the impact of GHG explains most of the temperature difference between K115 and K229 (cf. Fig. 5l with Fig. 5f).

While GHG have a homogeneous impact on Northern Hemisphere mean annual temperature, the impact of orbital parameters shows a larger spatial variability (Figs. 5g–i). Groll et al. (2005) and Groll and Widmann (2006) suggest that the orbital configuration of the simulated time period determines the structure of temperature-related teleconnections in the northern high latitudes, specifically the Arctic Oscillation. According to Thompson and Wallace (1998), the first mode of the empirical orthogonal functions (EOFs) of winter sea level pressure [December–March (DJFM)] over the 20°–90°N area gives a representation of the Arctic Oscillation (AO). We thus follow their method and, in order to understand how much of the temperature difference attributed to orbital parameters are related to the AO, we additionally regress winter air temperature on the principal component of the leading mode of sea level pressure EOF1 (PC1). EOF1 calculations are performed for MIS7_GHG and $MIS5_{FULL}$ experiments in order to compare with Figs. 5g–i.

In K239_GHG, K236_GHG, and K229_GHG, the Arctic Oscillation explains, 26.7%, 30.4%, and 31.9% of the variance in sea level pressure, respectively, while in K125, K122, and K115, it explains 29.1%, 25.8%, and 27.6% of the variance, respectively. The regressed winter air temperature spatial patterns are similar in K239_GHG, K236_GHG, K125, and K122, with positive temperatures located over Scandinavia, Siberia, and North America and negative temperatures located over southwest Greenland, Alaska, and east Siberia typical of a positive phase of the AO (PC1 is mostly positive; Figs. 6a–f). Comparably, the regressed winter air temperature spatial patterns are similar in both glacial inception experiments K229_GHG and K115, with negative temperatures located over Scandinavia, Russia, and North America and positive temperatures over southwest Greenland, Alaska, and east Siberia, typical of a negative phase of the AO (PC1 is mostly negative; Figs. 6c,f).

The comparison between winter temperature anomaly and temperature related to the Arctic Oscillation (regressed on the leading mode of EOF1) shows that most of the winter temperature difference between MIS7_GHG and $MIS5_{FULL}$ is related to the Arctic Oscillation (Fig. 6). In particular, the spatial patterns of regressed winter temperature difference (Figs. 6g–i) match almost perfectly those related to the Arctic Oscillation (Figs. 6j–l) for K239, K236, K125, and K122. While the amplitude of both temperature differences are similar between K239_GHG and K125, this is not the case between K236_GHG and K122, for which the winter temperature differences are smaller than those resulting from the Arctic Oscillation. The comparison between K229_GHG and K115 shows that the AO is closely related to the cooling over North America, while its influence is lower over Eurasia. The winter temperature differences are indeed larger than the regressed ones. Nevertheless, the Arctic Oscillation influences the spatial distribution of the mean annual temperature difference due to orbital forcing (Figs. 5j–l).

To summarize the contribution of GHG and orbital parameters to the temperature differences between MIS 7 and MIS 5 time slices, we averaged air temperature over Eurasia and North America in the latitude band 40°–70°N (the Arctic Ocean is excluded from computations). Those two regions are, indeed, of direct interest in the framework of glacial inception since their Arctic margins start to glaciate first. We plotted the separated contribution of GHG and orbital parameters to mean annual, winter, and summer temperatures differences between MIS 7 and MIS 5 (Fig. 7). The regional comparison reveals that, over Eurasia, the contribution of orbital parameters to the temperature difference between MIS 7 and MIS 5 is positive during winter and negative during summer in both K239 and K236 (Fig. 7a). While this contribution is compensated for by the impact of the low GHG values during winter, the orbital parameters dominate the summer temperature difference. In all the MIS 7 experiments, the large seasonal contrast resulting from the orbital parameters is compensated for during the year and, on mean annual basis, the low GHG values explain most of the difference between MIS 7 and MIS 5 (Fig. 7a). Note that during summer, the difference between K229 and K115

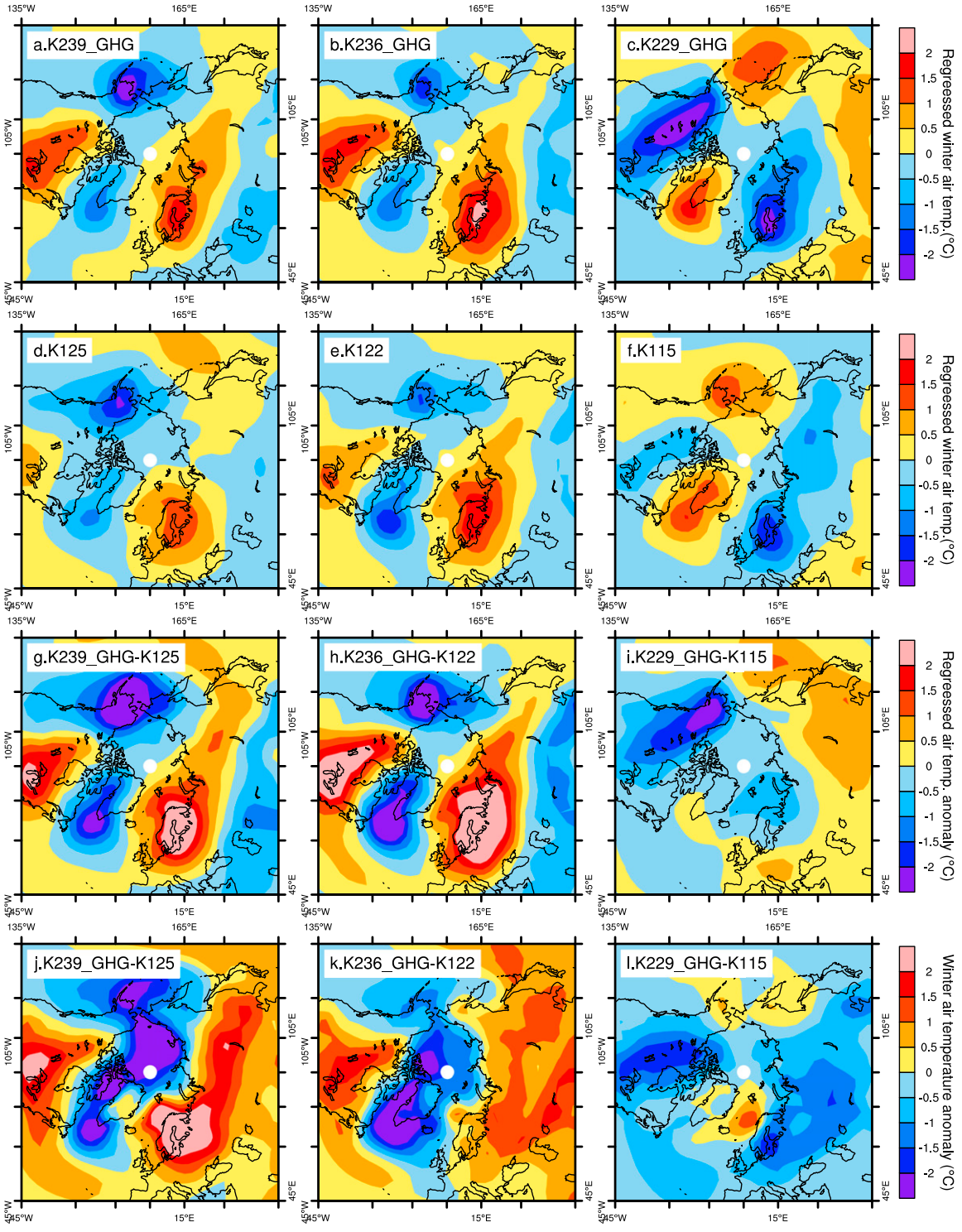

FIG. 6. Comparison between winter air temperature difference induced by orbital parameters and winter air temperature difference induced by the Arctic Oscillation. (a)–(c) Winter air temperature (DJFM) of MIS7_GHG simulations regressed on leading mode of EOF1 winter sea level pressure for each experiment (°C). The leading mode of sea level pressure (Arctic Oscillation) for winter months (DJFM) was calculated following Thompson and Wallace (1998). (d)–(f) As in (a)–(c), but for $MIS5_{FULL}$ experiments. (g)–(i) Regressed winter air temperature difference between MIS7_GHG and $MIS5_{FULL}$ simulations. (j)–(l) Winter air temperature (DJFM) difference between MIS7_GHG and $MIS5_{FULL}$ experiments (°C). The percentages of the contribution of the Arctic Oscillation to the nonseasonal variance of Northern Hemisphere sea level pressure for each experiment is of 26.7% for K239_GHG, 30.4% for K236_GHG, 31.9% for K229_GHG, 29.1% for K125, 27.6% for K122, and 25.8% for K115.

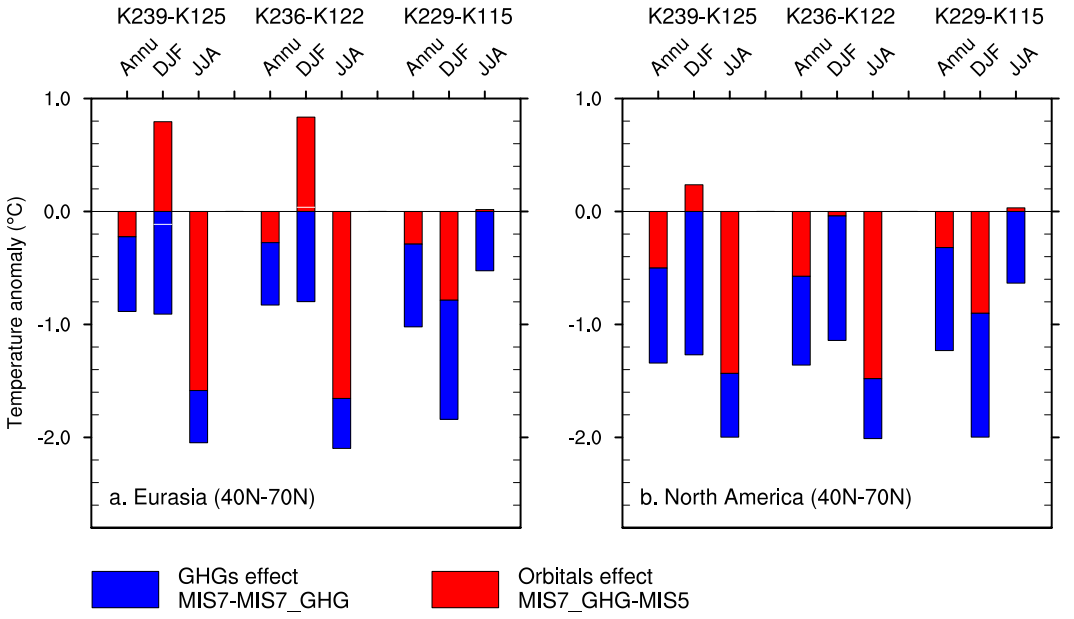

FIG. 7. Air temperature difference between $MIS7_{FULL}$ and $MIS5_{FULL}$ experiments (see Figs. 5d–l) divided in contribution of GHG (blue; $MIS7_{FULL}$ − MIS7_GHG experiments) and orbital parameters (red; MIS7_GHG − $MIS5_{FULL}$ experiments): averaged air temperature over (a) Eurasia and (b) North America. Since GHG and orbital parameters have an opposite effect on temperature for winter K239 − K125 and K236 − K122 in Eurasia, we represent the total difference between $MIS7_{FULL}$ and $MIS5_{FULL}$ with a white thin line. This means that, during winter, K239 − K125 is dominated by GHG contribution, while K236 − K122 is slightly more dominated by the impact of orbital parameters.

only results from K229 low GHG values (Fig. 7a). In contrast, North America seems less sensitive to the seasonal cycle than Eurasia and the contribution of orbital parameters to the temperature difference is generally of the same amplitude than over Eurasia (Fig. 7b). The only difference resides in K239 and K236 winter temperature difference, which is explained by the low MIS 7 GHG values exclusively, in contrast with Eurasia. Over both North America and Eurasia, GHG contribution varies between winter and summer but much less than the orbital parameters contribution. Note that, for the glacial inception simulation K229, the summer temperature difference with K115 results only from the impact of GHG over both regions.

The total mean annual temperature difference between $MIS7_{FULL}$ and $MIS5_{FULL}$ is about 0.5°C lower over North America than over Eurasia. The contribution of orbital parameters to this difference is larger over North America than over Eurasia. Despite those regional discrepancies, GHGs are undoubtedly responsible for most of the mean annual temperature difference between $MIS7_{FULL}$ and $MIS5_{FULL}$. In summary, the difference in mean annual air temperature between MIS 7 and MIS 5 results primarily from the low MIS 7 GHG and less from the difference in insolation between MIS 7 and MIS 5.

c. *Impact of GHG and orbital parameters on perennial snow*

In the previous section, the simulations show that during MIS 7, Northern Hemisphere mean annual temperature is colder by about 1.5°–3°C relatively to MIS 5 (Figs. 5d–f) and that this difference mostly results from the particularly low MIS 7 GHG concentrations. In this section, we investigate the impact of the mean annual temperature difference between the two periods on the timing and intensity of MIS 7 glacial inception. The amount of perennial snow cover accumulated in each experiment represents a good indicator of glacial inception. The astronomical theory of ice ages (Milankovitch 1941) states that cold summers are essential to maintain the perennial snow cover over Northern Hemisphere high latitudes, which in turn is essential to initiate a glaciation. In addition, Kageyama et al. (2004) show that mean annual temperature and snowfall are important to set the timing and the intensity of a glacial inception. Therefore, the difference in the mean annual temperature signal described above between our experiments might translate into perennial snow differences (Fig. 8).

For $MIS5_{FULL}$ experiments, K125 exhibits the smallest perennial snow cover (residence time of 365 days), as expected from the warmest among our set of simulations

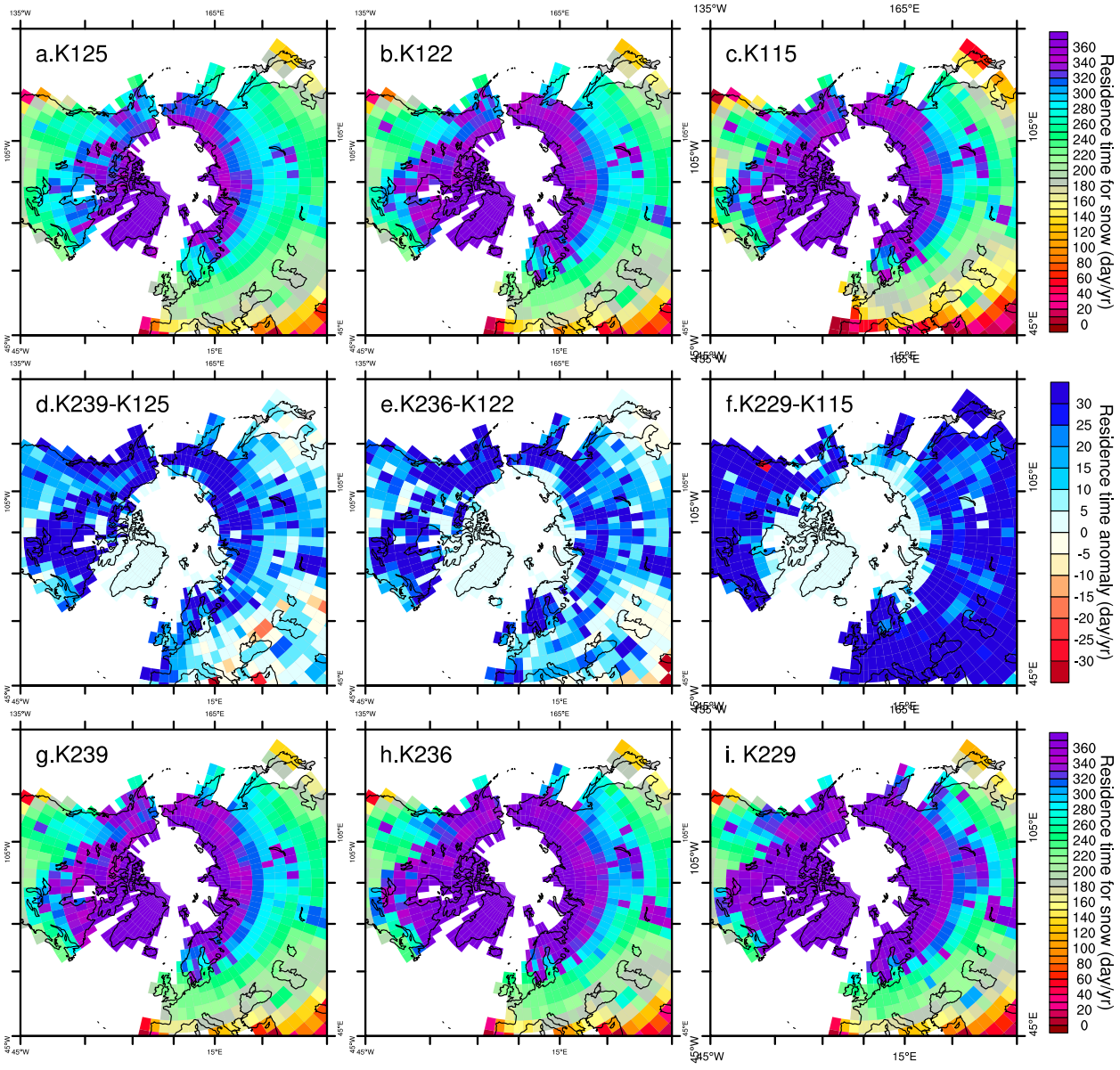

FIG. 8. (a)–(c) Residence time of snow cover (day yr^{-1}) for the $MIS5_{FULL}$ experiments, (d)–(f) difference in residence time between the $MIS7_{FULL}$ and $MIS5_{FULL}$ experiments, and (g)–(i) residence time of snow cover for the $MIS7_{FULL}$ experiments.

(Fig. 8a, dark purple). Some perennial snow is still visible over the Eurasian Arctic islands, while only a little perennial snow accumulates over the Canadian Archipelago. Perennial snow cover slightly expands in K122 while evolving toward the glacial inception (Fig. 8b), because of colder summer temperatures. As expected for a glacial inception climate, K115 exhibits an extensive perennial snow cover all along the Eurasian continental Arctic margins, on Svalbard, on the islands of the Barents and Kara Seas, and on the Canadian Archipelago (Fig. 8c). K115 has the coldest summers of all $MIS5_{FULL}$ simulations (Fig. 3), and therefore snowmelt is reduced during summer.

In line with $MIS5_{FULL}$ experiments, K239 exhibits the smallest MIS 7 perennial snow cover (Fig. 8g, dark purple). However, in contrast with K125, the perennial snow cover accumulates along the Arctic margins. The well-developed perennial snow cover expands in K236 and expands farther southward and eastward in K229, the glacial inception simulation (Figs. 8h,i). Compared to $MIS5_{FULL}$, in $MIS7_{FULL}$ the residence time for snow is longer by about 10–35 days over the Northern

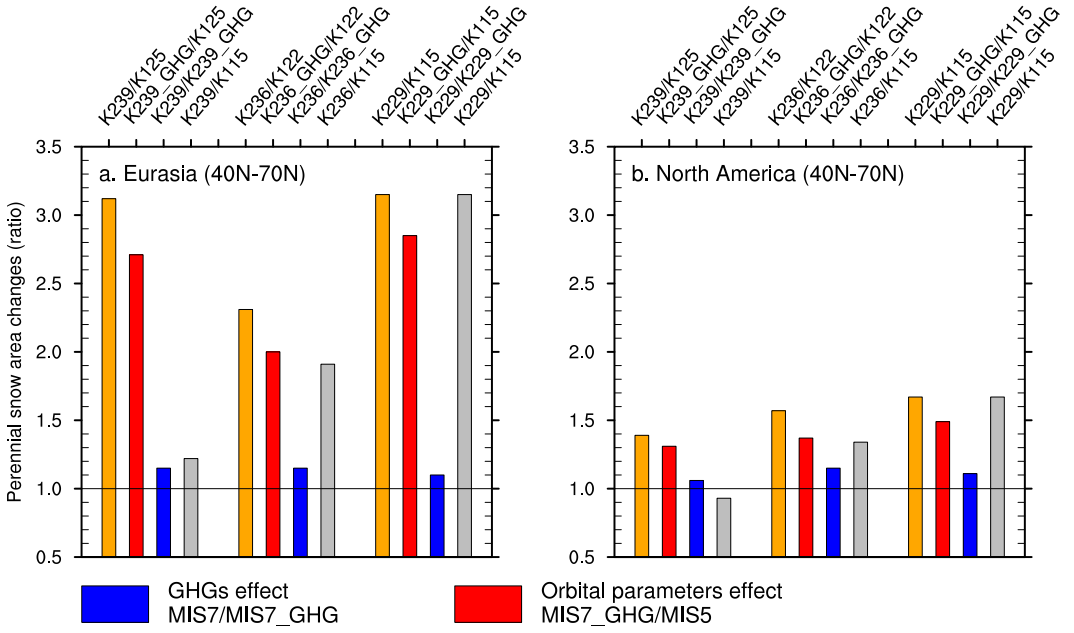

FIG. 9. Perennial snow-cover area changes (ratio; dimensionless) between the $MIS7_{FULL}$ and $MIS5_{FULL}$ experiments (orange). Red and blue bars correspond to the impact of orbital parameters and GHG on the perennial snow-cover area, respectively. Note that the multiplication of the red bars by the blue bars corresponds to the ratio between the $MIS7_{FULL}$ and $MIS5_{FULL}$ experiments. Finally, the ratio between the $MIS7_{FULL}$ experiments and the $MIS5_{FULL}$ glacial inception simulation K115 is represented in gray.

Hemisphere high latitudes (Figs. 8d,e). While the snow persists for a longer time only along the Arctic margins in K239 and in K236, the residence time for snow increases dramatically by more than 30 days over the whole Northern Hemisphere middle to high latitudes in K229 with respect to K115 (Fig. 8f).

Compared to $MIS5_{FULL}$, the increase in perennial snow area in $MIS7_{FULL}$ is 3 times larger over Eurasia in K239 and K229 and more than 2 times larger in K236 (Fig. 9a, orange bars). The expansion is more limited over North America and ranges from 40% to 70% (Fig. 9b, orange bars). On annual basis, most of this expansion is mostly explained by MIS 7 orbital configuration (Fig. 9, red bars). This contrasts with the fact that MIS 7 GHGs are responsible for most of the difference in mean annual temperature between MIS 7 and MIS 5 (Fig. 9, red bars). The expansion of the perennial snow cover due to the impact of GHG over the Northern Eurasia and North America is about 15% only, which in proportion represents approximately 33% of the total expansion over North America but only a 10% over Eurasia (Fig. 9, blue bars). To explain this discrepancy, we consider the spatial distribution of the mean annual snowfall due to MIS 7 orbital parameters and MIS 7 GHG, respectively (Fig. 10). The comparison between both impacts reveals that some spatial compensations occur at regional scale. The comparison between $MIS7_{FULL}$ and $MIS5_{FULL}$ experiments shows that, in K239 and in K236, mean annual snowfall is larger by about 10% along the Arctic margins (Figs. 10d,e). This increase results mainly from the impact of K239 and K236 orbital parameters (Figs. 10g,h).

The comparison between K229 and K115 shows that mean annual snowfall over Scandinavia and over the Russian Arctic margins decreases of about 6% whereas, along the Scandinavian Arctic margins and over east Siberia, it increases by about the same amount (Fig. 10f). Over western Eurasia, the larger amount of snowfall results from the impact of MIS 7 GHG, which is not totally compensated for by the orbital parameters decreases (Figs. 10i,l). On the contrary, over east Siberia, the increase of snowfall resulting from K229 orbital parameters is by far larger than the decrease caused by K229 GHG (Figs. 10i,l). Therefore, in proportion, over Eurasia, the impact of K229 orbital parameters on snowfall is larger than the impact of K229 GHG. This explains why, in K229, the expansion of the perennial snow cover is mainly due to orbital parameters (Fig. 9, red bars). We conclude that the small contribution of GHG to the expansion of the perennial snow cover is explained 1) by the relatively small mean annual cooling induced by MIS 7 GHG over Eurasia and North America, of about 1.5°C, which is probably not enough to substantially shift the 0°C summer temperature

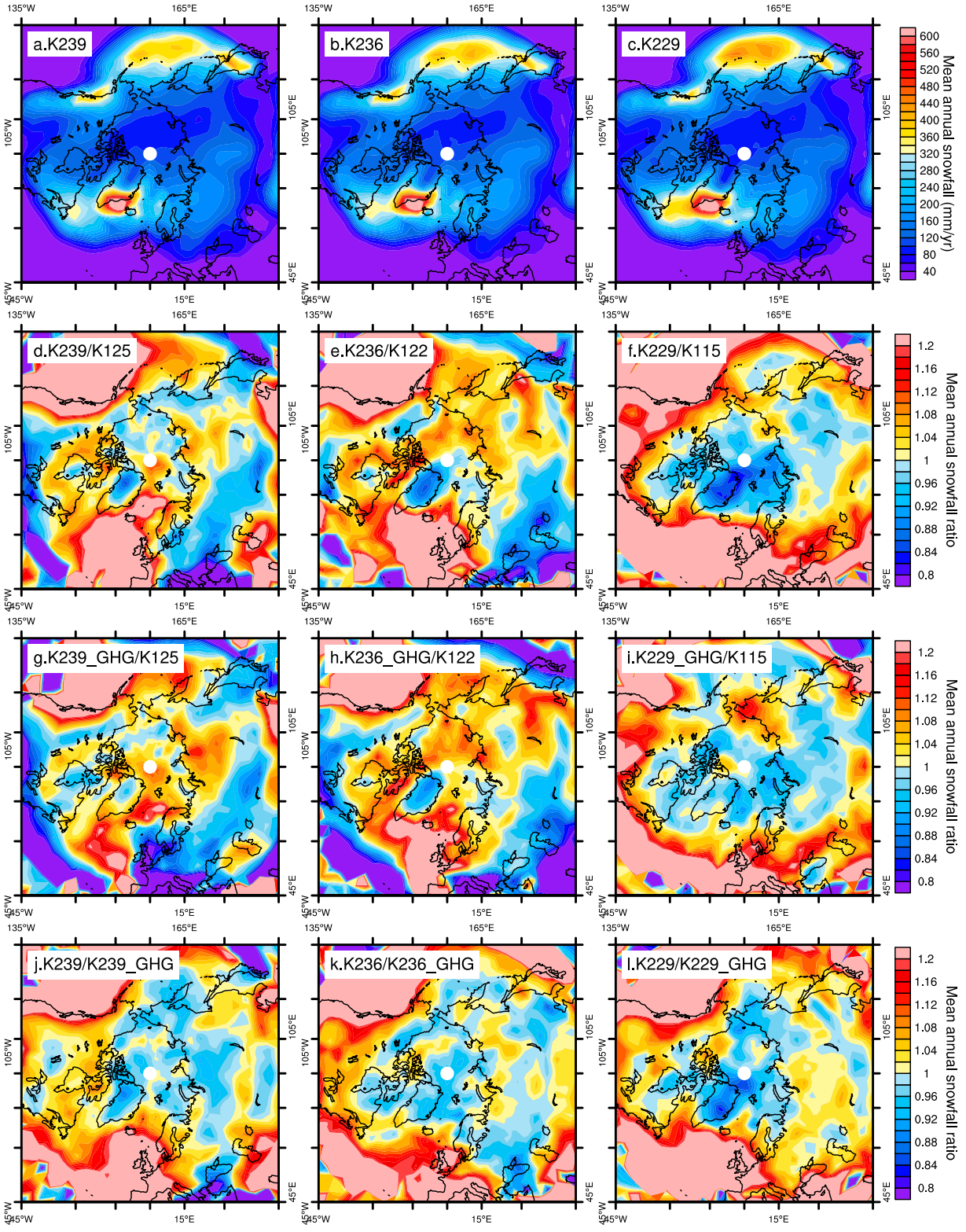

FIG. 10. Mean annual snowfall rates comparison between MIS 7 and MIS 5: (a)–(c) mean annual snowfall rates for $MIS7_{FULL}$ experiments ($mm\,yr^{-1}$); (d)–(f) ratio between $MIS7_{FULL}$ and $MIS5_{FULL}$ experiments; (g)–(i) impact of orbital parameters on snowfall (dimensionless; MIS7_GHG/$MIS5_{FULL}$ experiments); and (j)–(l) impact of GHG on snowfall (dimensionless; $MIS7_{FULL}$/MIS7_GHG experiments).

isotherm farther to the south and to induce large changes in the extent of MIS 7 perennial snow, and 2) by the spatial compensation occurring with MIS 7 orbital parameters.

Finally, compared to the glacial inception simulation K115, the perennial snow cover that accumulates in all $MIS7_{FULL}$ experiments is much larger, even in K239 (except over North America), which represents the interglacial simulation of $MIS7_{FULL}$. In K239, the perennial snow area is larger than in K115 by about 20% over Eurasia, 2 times larger in K236 and 3 times larger in K229 (Fig. 9). Over North America, the perennial snow area is reduced by about 10% in K239 compared to K115, larger by about 40% in K236, and larger by 60% in K229 (Fig. 9). This is a remarkable result which suggests that MIS 7 cold climate allows for a particularly fast accumulation of a perennial snow cover right after the peak interglacial that occurred toward 245 kyr.

4. Conclusions

In this work we compare the climate of MIS 5 and MIS 7 time periods by simulating the mean climate states of six time slices at 115, 122, 125, 229, 236, and 239 kyr in addition to three other simulations orbitally set with MIS 7 values but using MIS 5 GHG values. Paleo data suggest that MIS 7 interglacial was short compared to MIS 5 interglacial (Tzedakis et al. 2012). In fact, GHG abruptly dropped immediately after the peak interglacial toward 245 kyr, while it happens ≈20 kyr after MIS 5 peak interglacial. Our experiments were designed to investigate the impact of GHG on the timing and intensity of glacial inception and are summarized in Table 1. By comparing MIS 7 and MIS 5 mean climate states, our results show that the following:

- MIS 7 is generally colder over the Northern Hemisphere than MIS 5. On annual basis MIS 7 lower GHG explains more than 70% of the boreal lands temperature discrepancy between MIS 5 and MIS 7 and 100% in the case of MIS 7 glacial inception (229 kyr). On a seasonal basis, the impact of orbital parameters can be stronger than the effect of GHG but are compensated for on an annual basis and results are smaller than the impact of GHG.
- The Arctic Oscillation explains most of the winter temperature difference between MIS 7 and MIS 5 resulting from the impact of orbital parameters.
- All MIS 7 simulations exhibit a perennial snow cover that is larger than in the MIS 5 glacial inception simulation. Contrary to air surface temperature, the difference between MIS 7 and MIS 5 perennial snow-cover area is controlled by the orbital parameters, enhanced by the cooling effect of MIS 7 low GHG. This is because spatial compensations in mean annual snowfall occur between orbital parameters and GHG.
- Eurasian perennial snow cover is more sensitive to the low MIS 7 temperature, and results in a perennial snow area are 3 times larger than in the MIS 5 experiments.

Based on those results, we suggest that MIS 7 glacial inception probably started few thousand years after the peak interglacial, while during MIS 5 both proxies and simulations suggest that the glacial inception started only ≈10 kyr after the peak of the interglacial.

Finally, Eurasia presents the strongest response to MIS 7 external forcing and low GHG, which indicates that the glacial inception is more favorable over this area than over North America when GHGs are particularly low. This is supported by Bonelli et al. (2009), who showed that for MIS 5 glacial inception Eurasian ice sheet starts developing only after GHG have decreased significantly. The larger sensitivity of Eurasia also implies that interglacials as cold as or colder than MIS 7 (i.e., pre-MBE interglacials) could be more favorable to glacial inception over Eurasia in general.

Acknowledgments. We gratefully acknowledge the support of Italian Ministry of Education, University and Research and Ministry for Environment, Land and Sea through the project GEMINA. We address a special thanks to members of the Past Interglacials (PIGS) working group of the Past Global Changes (PAGES) project for their support and feedback.

REFERENCES

Berger, A., 1978: Long-term variations of daily insolation and quaternary climatic changes. *J. Atmos. Sci.,* **35,** 2362–2367, doi:10.1175/1520-0469(1978)035<2362:LTVODI>2.0.CO;2.

Bintanja, R., R. S. van de Wal, and J. Oerlemans, 2005: Modelled atmospheric temperatures and global sea levels over the past million years. *Nature,* **437,** 125–128, doi:10.1038/nature03975.

Bonelli, S., S. Charbit, M. Kageyama, M.-N. Woillez, G. Ramstein, C. Dumas, and A. Quiquet, 2009: Investigating the evolution of major Northern Hemisphere ice sheets during the last glacial-interglacial cycle. *Climate Past,* **5,** 329–345, doi:10.5194/cp-5-329-2009.

Calov, R., A. Ganopolsi, V. Petoukhov, M. Claussen, V. Brovkin, and C. Kutbatzki, 2005: Transient simulation of the last glacial inception. Part II: Sensitivity and feedback analysis. *Climate Dyn.,* **24,** 563–576, doi:10.1007/s00382-005-0008-5.

Colleoni, F., S. Masina, A. Cherchi, A. Navarra, C. Ritz, V. Peyaud, and B. Otto-Bliesner, 2014: Modeling Northern Hemisphere ice-sheet distribution during MIS 5 and MIS 7 glacial inceptions. *Climate Past,* **10,** 269–291, doi:10.5194/cp-10-269-2014.

Dahl-Jensen, D., and Coauthors, 2013: Eemian interglacial reconstructed from a Greenland folded ice core. *Nature,* **493,** 489–494, doi:10.1038/nature11789.

Dutton, A., E. Bard, F. Antonioli, T. M. Esat, K. Lambeck, and M. T. McCulloch, 2009: Phasing and amplitude of sea-level

and climate change during the penultimate interglacial. *Nat. Geosci.,* **2,** 355–359, doi:10.1038/ngeo470.

Gent, P. R., and Coauthors, 2011: The Community Climate System Model version 4. *J. Climate,* **24,** 4973–4991, doi:10.1175/2011JCLI4083.1.

Groll, N., and M. Widmann, 2006: Sensitivity of temperature teleconnections to orbital changes in AO-GCM simulations. *Geophys. Res. Lett.,* **33,** L12705, doi:10.1029/2005GL025578.

——, ——, J. M. Jones, F. Kaspar, and S. J. Lorenz, 2005: Simulated relationships between regional temperatures and large-scale circulation: 125 kyr BP (Eemian) and the preindustrial period. *J. Climate,* **18,** 4032–4045, doi:10.1175/JCLI3469.1.

Haug, G. H., and Coauthors, 2005: North Pacific seasonality and the glaciation of North America 2.7 million years ago. *Nature,* **433,** 821–825, doi:10.1038/nature03332.

Helmke, J. P., H. A. Bauch, and H. Erlenkeuser, 2003: Development of glacial and interglacial conditions in the Nordic Seas between 1.5 and 0.35 Ma. *Quat. Sci. Rev.,* **22,** 1717–1728, doi:10.1016/S0277-3791(03)00126-4.

Jansen, J., A. Kuijpers, and S. Troelstra, 1986: A mid-Brunhes climatic event: Long-term changes in global atmosphere and ocean circulation. *Science,* **232,** 619–622, doi:10.1126/science.232.4750.619.

Jochum, M., A. Jahn, S. Peacock, D. A. Bailey, J. Fasullo, J. Kay, S. Levis, and B. Otto-Bliesner, 2012: True to Milankovitch: Glacial inception in the new Community Climate System Model. *J. Climate,* **25,** 2226–2239, doi:10.1175/JCLI-D-11-00044.1.

Johnsen, S., and Coauthors, 2001: Oxygen isotope and palaeotemperature records from six Greenland ice-core stations: Camp Century, Dye-3, GRIP, GISP2, Renland and NorthGRIP. *J. Quat. Sci.,* **16,** 299–307, doi:10.1002/jqs.622.

Jouzel, J., and Coauthors, 2007: Orbital and millennial Antarctic climate variability over the past 800,000 years. *Science,* **317,** 793–797, doi:10.1126/science.1141038.

Kageyama, M., S. Charbit, C. Ritz, M. Khodri, and G. Ramstein, 2004: Quantifying ice-sheet feedbacks during the last glacial inception. *Geophys. Res. Lett.,* **31,** L24203, doi:10.1029/2004GL021339.

Kawamura, K., and Coauthors, 2007: Northern Hemisphere forcing of climatic cycles in Antarctica over the past 360,000 years. *Nature,* **448,** 912–916, doi:10.1038/nature06015.

Kubatzki, C., M. Claussen, R. Calov, and A. Ganopolski, 2006: Sensitivity of the last glacial inception to initial and surface conditions. *Climate Dyn.,* **27,** 333–344, doi:10.1007/s00382-006-0136-6.

Lang, N., and E. W. Wolff, 2011: Interglacial and glacial variability from the last 800 ka in marine, ice and terrestrial archives. *Climate Past,* **7,** 361–380, doi:10.5194/cp-7-361-2011.

Lisiecki, L., and M. Raymo, 2005: A Pliocene-Pleistocene stack of 57 globally distributed benthic $\delta^{18}O$ records. *Paleoceanography,* **20,** PA1003, doi:10.1029/2004PA001071.

——, and ——, 2007: Pliopleistocene climate evolution: Trends and transitions in glacial cycle dynamics. *Quat. Sci. Rev.,* **26,** 56–69, doi:10.1016/j.quascirev.2006.09.005.

Loulergue, L., and Coauthors, 2008: Orbital and millennial-scale features of atmospheric CH_4 over the past 800,000 years. *Nature,* **453,** 383–386, doi:10.1038/nature06950.

Luthi, D., and Coauthors, 2008: High-resolution carbon dioxide concentration record 650,000–800,000 years before present. *Nature,* **453,** 379–382, doi:10.1038/nature06949.

Milankovitch, M., 1941: *Kanon der Erdbestrahlung und seine Andwendung auf das Eiszeitenproblem.* Royal Serbian Academy, 633 pp.

Mudelsee, M., and M. E. Raymo, 2005: Slow dynamics of the Northern Hemisphere glaciations. *Paleoceanography,* **20,** PA4022, doi:10.1029/2005PA001153.

Rohling, E., K. Grant, M. Bolshaw, A. Roberts, M. Siddall, C. Hemleben, and M. Kucera, 2009: Antarctic temperature and global sea level closely coupled over the past five glacial cycles. *Nat. Geosci.,* **2,** 500–504, doi:10.1038/ngeo557.

Schilt, A., M. Baumgartner, T. Blunier, J. Schwander, R. Spahni, H. Fischer, and T. Stocker, 2010: Glacial-interglacial and millennial scale variations in the atmospheric nitrous oxide concentration during the last 800,000 years. *Quat. Sci. Rev.,* **29,** 182–192, doi:10.1016/j.quascirev.2009.03.011.

Shields, C. A., D. A. Bailey, G. Danabasoglu, M. Jochum, J. T. Kiehl, S. Levis, and S. Park, 2012: The low-resolution CCSM4. *J. Climate,* **25,** 3993–4014, doi:10.1175/JCLI-D-11-00260.1.

Siddall, M., E. Bard, E. J. Rohling, and C. Hemleben, 2006: Sea-level reversal during termination II. *Geology,* **34,** 817–820, doi:10.1130/G22705.1.

Thompson, D. W., and J. M. Wallace, 1998: The Arctic Oscillation signature in the wintertime geopotential height and temperature fields. *Geophys. Res. Lett.,* **25,** 1297–1300, doi:10.1029/98GL00950.

Tzedakis, P., J. Channell, D. Hodell, H. Kleiven, and L. Skinner, 2012: Determining the natural length of the current interglacial. *Nat. Geosci.,* **5,** 138–141, doi:10.1038/ngeo1358.

Vettoretti, G., and W. R. Peltier, 2003: Post-Eemian glacial inception. Part I: The impact of summer seasonal temperature bias. *J. Climate,* **16,** 889–911, doi:10.1175/1520-0442(2003)016<0889:PEGIPI>2.0.CO;2.

Wang, Z., and L. Mysak, 2002: Simulation of the last glacial inception and rapid ice sheet growth in the McGill paleoclimate model. *Geophys. Res. Lett.,* **29,** 2102, doi:10.1029/2002GL015120.

Yeager, S. G., C. A. Shields, W. G. Large, and J. J. Hack, 2006: The low-resolution CCSM3. *J. Climate,* **19,** 2545–2566, doi:10.1175/JCLI3744.1.

Yin, Q., and A. Berger, 2012: Individual contribution of insolation and CO_2 to the interglacial climates of the past 800,000 years. *Climate Dyn.,* **38,** 709–724, doi:10.1007/s00382-011-1013-5.